

# Phase sensitive properties and coherent manipulation of a photonic crystal microcavity

WADIM QUIRING,<sup>1,\*</sup> BJÖRN JONAS,<sup>1</sup> JENS FÖRSTNER,<sup>2</sup> ASHISH K. RAI,<sup>3</sup>  
DIRK REUTER,<sup>1</sup> ANDREAS D. WIECK,<sup>3</sup> AND ARTUR ZRENNER<sup>1</sup>

<sup>1</sup>Physics Department and Center for Optoelectronics and Photonics Paderborn (CeOPP), Universität Paderborn, Warburger Straße 100, Paderborn 33098, Germany

<sup>2</sup>Department of Electrical Engineering and Center for Optoelectronics and Photonics Paderborn (CeOPP), Universität Paderborn, Warburger Straße 100, Paderborn 33098, Germany

<sup>3</sup>Lehrstuhl für Angewandte Festkörperphysik, Ruhr-Universität Bochum, Universitätsstraße 150, Bochum D-44780, Germany

\*wadim.quiring@upb.de

**Abstract:** We present phase sensitive cavity field measurements on photonic crystal microcavities. The experiments have been performed as autocorrelation measurements with ps double pulse laser excitation for resonant and detuned conditions. Measured E-field autocorrelation functions reveal a very strong detuning dependence of the phase shift between laser and cavity field and of the autocorrelation amplitude of the cavity field. The fully resolved phase information allows for a precise frequency discrimination and hence for a precise measurement of the detuning between laser and cavity. The behavior of the autocorrelation amplitude and phase and their detuning dependence can be fully described by an analytic model. Furthermore, coherent control of the cavity field is demonstrated by tailored laser excitation with phase and amplitude controlled pulses. The experimental proof and verification of the above described phenomena became possible by an electric detection scheme, which employs planar photonic crystal microcavity photo diodes with metallic Schottky contacts in the defect region of the resonator. The applied photo current detection was shown to work also efficiently at room temperature, which make electrically contacted microcavities attractive for real world applications.

©2016 Optical Society of America

OCIS codes: (250.0250) Optoelectronics; (040.0040) Detectors; (160.5298) Photonic crystals.

## References and links

1. H. Sekoguchi, Y. Takahashi, T. Asano, and S. Noda, "Photonic crystal nanocavity with a Q-factor of ~9 million," *Opt. Express* **22**(1), 916–924 (2014).
2. D. Wang, Z. Yu, Y. Liu, X. Guo, C. Shu, S. Zhou, and J. Zhang, "Ultrasmall modal volume and high Q factor optimization of a photonic crystal slab cavity," *J. Opt.* **15**(12), 125102 (2013).
3. M. Boroditsky, R. Coccioli, E. Yablonovitch, Y. Rahmat-Samii, and K. W. Kim, "Smallest possible electromagnetic mode volume in a dielectric cavity," *IEE Proc., Optoelectron.* **145**(6), 391–397 (1998).
4. E. M. Purcell, "Spontaneous emission probabilities at radio frequencies," *Phys. Rev.* **69**, 681 (1946).
5. K. J. Vahala, "Optical microcavities," *Nature* **424**(6950), 839–846 (2003).
6. Y. Zhang, Y. Zhao, and R. Lv, "A review for optical sensors based on photonic crystal cavities," *Sens. Actuators A Phys.* **233**, 374–389 (2015).
7. B. Wild, R. Ferrini, R. Houdré, M. Mulot, S. Anand, and C. J. M. Smith, "Temperature tuning of the optical properties of planar photonic crystal microcavities," *Appl. Phys. Lett.* **84**(6), 846 (2004).
8. D. Sridharan, E. Waks, G. Solomon, and J. T. Fourkas, "Reversible tuning of photonic crystal cavities using photochromic thin films," *Appl. Phys. Lett.* **96**(15), 153303 (2010).
9. T.-W. Lu and P.-T. Lee, "Ultra-high sensitivity optical stress sensor based on double-layered photonic crystal microcavity," *Opt. Express* **17**(3), 1518–1526 (2009).
10. R. Perahia, J. D. Choen, S. Meenehan, T. P. Mayer Alegre, and O. Painter, "Electrostatically tunable optomechanical "zipper" cavity laser," *Appl. Phys. Lett.* **97**(19), 191112 (2010).
11. L. Midolo, S. N. Yoon, F. Pagliano, T. Xia, F. W. M. van Otten, M. Lerner, S. Höfling, and A. Fiore, "Electromechanical tuning of vertically-coupled photonic crystal nanobeams," *Opt. Express* **20**(17), 19255–19263 (2012).

12. M. W. McCutcheon, A. G. Pattantyus-Abraham, G. W. Rieger, and J. F. Young, "Emission spectrum of electromagnetic energy stored in a dynamically perturbed optical microcavity," *Opt. Express* **15**(18), 11472–11480 (2007).
13. J. Upham, H. Inoue, Y. Tanaka, W. Stumpf, K. Kojima, T. Asano, and S. Noda, "Pulse capture without carrier absorption in dynamic Q photonic crystal nanocavities," *Opt. Express* **22**(13), 15459–15466 (2014).
14. T. J. Karle, F. Raineri, V. Roppo, F. Bordas, P. Monnier, S. Ali, I. Sivan, and R. Raj, "Temporal ringdown of silicon-on-insulator racetrack resonators," *Opt. Lett.* **38**(13), 2304–2306 (2013).
15. T. Asano, B.-S. Song, Y. Akahane, and S. Noda, "Ultra-high-Q nanocavities in two-dimensional photonic crystal slabs," *IEEE J. Sel. Top. Quantum Electron.* **12**, 1123–1134 (2006).
16. W. Quiring, M. Al-Hmoud, A. Rai, D. Reuter, A. D. Wieck, and A. Zrenner, "Photonic crystal cavities with metallic Schottky contacts," *Appl. Phys. Lett.* **107**(4), 41113 (2015).
17. D. Marcuse, "Coupled mode theory of optical resonant cavities," *IEEE J. Quantum Electron.* **21**(11), 1819–1826 (1985).
18. H. A. Haus and W. Huang, "Coupled-mode theory," *Proc. IEEE* **79**(10), 1505–1518 (1991).
19. J. D. Gaskill, *Linear Systems, Fourier Transforms and Optics* (Wiley, 1978).
20. G. Vincent, A. Chantre, and D. Bois, "Electric field effect on the thermal emission of traps in semiconductor junctions," *J. Appl. Phys.* **50**(8), 5484 (1979).
21. P. W. Fry, I. E. Itskevich, S. R. Parnell, J. J. Finley, L. R. Wilson, K. L. Schumacher, D. J. Mowbray, M. S. Skolnick, M. Al-Khafaji, A. G. Cullis, M. Hopkinson, J. C. Clark, and G. Hill, "Photocurrent spectroscopy of InAs/GaAs self-assembled quantum dots," *Phys. Rev. B* **62**(24), 16784–16791 (2000).
22. M. Ohmori, P. Vitushinskiy, and H. Sakaki, "Diffusion process of excitons in the wetting layer and their trapping by quantum dots in sparsely spaced InAs quantum dot systems," *Appl. Phys. Lett.* **98**(13), 133109 (2011).
23. H. Hillmer, A. Forchel, S. Hansmann, M. Morohashi, E. Lopez, H. P. Meier, and K. Ploog, "Optical investigations on the mobility of two-dimensional excitons in GaAs/Ga<sub>1-x</sub>Al<sub>x</sub>As quantum wells," *Phys. Rev. B Condens. Matter* **39**(15), 10901–10912 (1989).
24. J. Baum, R. Tycko, and A. Pines, "Broadband and adiabatic inversion of a two-level system by phase-modulated pulses," *Phys. Rev. A Gen. Phys.* **32**(6), 3435–3447 (1985).
25. E. R. Schmidgall, P. R. Eastham, and R. T. Phillips, "Population inversion in quantum dot ensembles via adiabatic rapid passage," *Phys. Rev. B* **81**(19), 195306 (2010).
26. C.-M. Simon, T. Belhadj, B. Chatel, T. Amand, P. Renucci, A. Lemaitre, O. Krebs, P. A. Dalgarno, R. J. Warburton, X. Marie, and B. Urbaszek, "Robust quantum dot exciton generation via adiabatic passage with frequency-swept optical pulses," *Phys. Rev. Lett.* **106**(16), 166801 (2011).

## 1. Introduction

Photonic crystal microcavities (PhCC) exhibit outstanding properties as for example very high Q-factors which allow to store the light up to several nanoseconds [1] or tiny mode volumes down to the range of  $\lambda^3$  [2,3]. Small mode volume and high Q-factor lead to a strongly enhanced light matter interaction [4], which makes PhCCs interesting for fundamental research as well as for applications [5,6]. In many cases also the dynamic control of cavity key properties is desired. Existing approaches employ for example the tuning of the resonance wavelength by temperature [7], the use of photochromic films on top of the samples [8] or coupled cavities with strain- [9] or electrostatic force-controlled [10,11] inter-cavity distance. A very promising technique for extremely fast dynamic control of the PhCC Q-factor by laser excitation and free carrier generation was demonstrated by McCutcheon et al. [12] and Upham et al. [13].

In the present work we have investigated the dynamics of the cavity field, performing phase sensitive measurements by two pulse excitation of a GaAs slab photonic crystal cavity. A proper adjustment of the pulse amplitudes and relative phase allows here for a detailed phase resolved analysis of the cavity excitation and for the coherent control of the cavity field on the time scale of the laser pulse duration.

In order to measure the dynamical cavity field response on a ps-time scale, methods like non-linear frequency mixing [14], time-correlated single-photon counting [15] or pump-probe experiments [12] have been used in the past. An alternative detection technique for the cavity field, which is used here, is the measurement of the autocorrelation function. For this we have developed PhCC Schottky photo diodes [16]. They allow for background free electric detection, which is a great advantage compared to established transmission or reflection measurements.

## 2. Investigated system

### 2.1 Sample design

The investigated sample is a GaAs slab based photonic crystal cavity with a narrow metallic Schottky contact located in the center of the defect (see Fig. 1(a)). The layer sequence of the 180 nm thick membrane consists of 50 nm  $n^+$  doped GaAs followed by 40 nm of i-GaAs, an InGaAs wetting layer (WL) and 90 nm of i-GaAs (see Fig. 1(a)). Together with the metal strip it forms a local n-i-Schottky diode, which is used here for photo current (PC) measurements in the cavity.

The PhCC is fabricated by e-beam lithography and reactive ion etching (see Ref [16]. for more details). The lattice constant of the PhCC is  $a = 250\text{ nm}$  and the hole radius is  $r \approx 0.25 \cdot a$ . The cavity defect is formed by a line of 15 missing holes (L15 cavity). The use of such a long cavity results in decreased radiative and scattering losses compared to shorter cavities with metal strip [16]. The fabricated strip is 50 nm wide and 10 nm thick (5 nm Chromium and 5 nm Gold). An SEM image of the fabricated structure is shown in Fig. 1(a).

### 2.2 Photocurrent spectroscopy

The described cavity design allows for absorption measurements by PC spectroscopy. The cavity mode spectrum can be monitored by sweeping the wavelength of a narrow band laser and measuring the corresponding PC [16]. The field enhancement at the cavity resonance leads to a corresponding enhancement of the PC signal. In this manner we obtain direct access to the intensity of the cavity excitation.

In the following we concentrate on the cavity mode with the highest Q-factor of around 5000. Its resonance energy of 1.29 eV (960 nm) is far away from the center of the WL absorption at 1.39 eV (at  $T = 4.2\text{ K}$ ). As the cavity resonance is located only in the band tail of the WL, its Q-factor is not limited by WL absorption but by other losses like fabrication imperfections and light scattering by the metal strip. The selected cavity mode is strongly polarization dependent and can be best excited by linear polarized light, oriented parallel to the metal strip.

### 2.3 ps-pulse excitation

For ps excitation we use a Titanium-Sapphire (Ti:Sa) laser with a repetition rate of 72 MHz and a pulse duration of  $t_{\text{pulse}} \approx 3.5\text{ ps}$ . The pulses have a  $\text{sech}^2$ -envelope and are Fourier limited.

The response of a micro-cavity, excited by a laser pulse depends on the pulse duration  $t_{\text{pulse}}$ , the cavity Q-factor and the detuning between laser and cavity resonance  $\omega_{\text{detuning}}$ . The time evolution of a slightly detuned laser-cavity system is shown in Figs. 1(c)-1(f). In Fig. 1(c) we show a schematic view of the laser field  $E_L$  and its envelope  $g_L$ . The excitation pulse is described as a harmonic oscillation (frequency  $\omega_L$ ), which is modulated by  $g_L$ . As an example, Fig. 1(d) shows a cavity response  $E_C$  and  $g_C$  for a slightly detuned excitation pulse ( $\omega_L > \omega_C$ ). The frequency of the cavity field is not constant over time.  $E_C$  starts to oscillate with the driving frequency of the excitation pulse  $\omega_L$  and changes slowly to the resonance frequency  $\omega_C$  after the pulse duration. Due to this frequency chirp it is beneficial for further discussions to change the reference frame to the rotating reference frame of the laser.

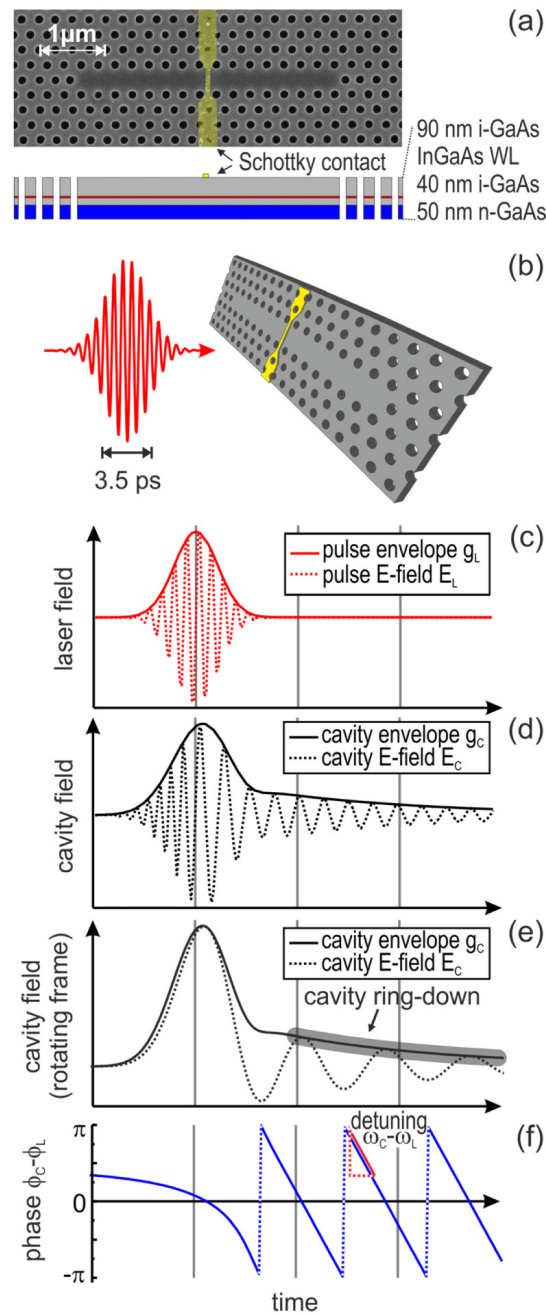


Fig. 1. (a) SEM image and schematic view of the investigated GaAs PhCC free standing membrane with metallic Schottky contact (highlighted for better contrast), (b) which is excited by a near-resonant (or resonant) ps-laser pulse. The n-i-Schottky photo diode is used for PC detection via WL band tail absorption. (c) E-field and corresponding envelope of the laser excitation pulse and (d) the resulting cavity response. The change of the carrier frequency versus time is a result of the detuning between cavity and laser. (e) Numeric results for the cavity response in the rotating reference frame of the laser field and (f) for the phase evolution of the cavity field in the rotation frame of the laser field.

We have modeled the system numerically with results shown in Figs. 1(e) and 1(f). For this we assumed that the WL is always excited in the linear regime and the measured signal is proportional to the excitation intensity  $I_C(\omega) \propto |E_C(\omega)|^2 \propto |E_L(\omega)|^2$ . The cavity mode is described as a dissipative oscillator with complex electric field amplitude  $E_C(t)$ , as  $E_L(t)$  considered in a rotating frame.  $E_C(t)$  satisfies the differential equation [17,18]

$$\dot{E}_C(t) = i\omega_{\text{detuning}} E_C(t) - \gamma E_C(t) + \mu_{\text{in}} E_L(t)$$

The detuning is given by  $\omega_{\text{detuning}} = \omega_C - \omega_L$ ,  $\gamma$  is the cavity field ring-down constant and  $\mu_{\text{in}}$  corresponds to the input coupling rate. An example for a cavity excited by a 3 ps pulse with detuning  $\omega_{\text{detuning}} = 700 \mu\text{eV}$  ( $\approx 0.5 \text{ nm}$ ) is shown in Fig. 1(d). The rotating frame representation nicely shows the changes of the cavity mode oscillation frequency. The corresponding envelope  $g_C = |E_C(t)|$  is not affected by the choice of the reference frame and is therefore equal to the envelope shown in Fig. 1(d). After the excitation pulse the regime of the exponential cavity ring down can be clearly seen (marked grey in Fig. 1(e)).

In Fig. 1(f) we further show the phase  $\phi = \phi_C - \phi_L$  between the cavity field  $E_C$  and laser field  $E_L$ . It is obtained by calculating the argument of the complex valued  $E_C(t)$ :  $\tan \phi = \text{Im}\{E_C(t)\} / \text{Re}\{E_C(t)\}$ . Before the pulse arrives, the phase is equal to  $\pi/2$ . It accelerates and finally, after the pulse duration, runs off with constant velocity. The constant slope of the phase function is equal to the detuning  $\omega_{\text{detuning}}$  between laser and cavity.

In our experiments, neither the fast oscillations nor the phase can be instantly measured due to the extremely short time scale. To get access to the phase we use the technique of two pulse interference.

### 3. Experimental method

#### 3.1 Experimental setup

The train of pulses from the Ti:Sa laser was split in two equal parts and combined again by a Michelson interferometer. In order to achieve a variable time delay  $t_{\text{delay}}$  between the pulses one interferometer end mirror was mounted on a combined positioner, which allows for coarse adjustment and additional fine tuning via a closed loop nano-positioner. An interference between the (partly) overlapping pulses could be observed for delay times of about two times the pulse duration. This correspond to a length of  $2l_{\text{pulse}} = 2c \cdot t_{\text{pulse}} \approx 2 \text{ mm}$ , where  $c$  is the speed of light in vacuum. The output signal of the interferometer was adjusted with respect to polarization and average power and was send through a polarization maintaining beam splitter. One part was used for the cavity excitation and another for a reference measurement of the laser interference by a power detector. The excitation light was focused on the sample by an objective lens (x100,  $NA = 0.75$ ) to a spot size of  $\approx 1 \mu\text{m}$ .

The experiments were performed at 4.2 K in a helium cryostat and at room temperature.

### 3.2 Measurement procedure

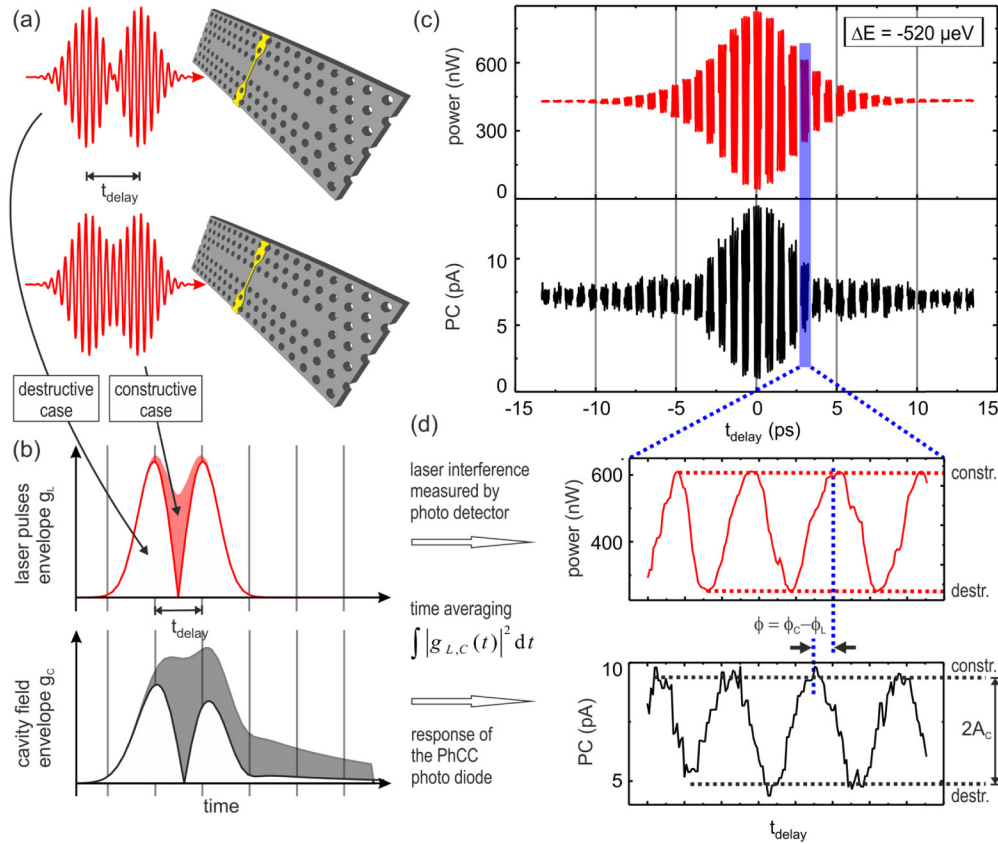


Fig. 2. (a) PhCC excited by two equal pulses with phase control by variable time delay  $t_{\text{delay}}$  yielding destructive (top) and constructive (bottom) interference. (b) Extracted envelope functions corresponding to constructive and destructive case for laser (red, the arrows from (a) indicate the link between E-field and envelope) and cavity response (black). (c) Experimentally obtained interference patterns for laser and cavity signal. (d) Detailed view of the measured time averaged signal for laser and cavity. The signals exhibit a phase shift  $\phi$ .

In the following we present our procedure for the measurement of the phase difference  $\phi = \phi_C - \phi_L$  between the cavity field  $E_C$  and the laser field  $E_L$ . A direct, time dependent observation like it is shown in Fig. 1(f) is not possible because of the fast field oscillations ( $\omega_L \approx 2\pi \cdot 310 \text{ THz}$ ). However, the phase  $\phi$  can be extracted by comparing the interference signals obtained from the PhCC photo diode and from the bare laser pulses. Both signals depend on the time delay  $t_{\text{delay}}$  between the two pulses. The cases of destructive and constructive interference are shown schematically in Fig. 2(a). The corresponding time dependent envelope functions for laser  $g_L$  and cavity signal  $g_C$  are plotted in Fig. 2(b). The interfering laser pulses produce a symmetric signal  $g_L$ , which is enhanced for the constructive case and offers a central dip for the destructive case. The cavity signal  $g_C$  is more complicated. It is asymmetric and shows in both cases a signature of the cavity ring-down, even when the laser pulses have already vanished. It is important to state, that in general, the laser and cavity fields are out of phase (see Fig. 1(f)) and e.g. a constructive interference of laser pulses does not automatically result in a constructive interference of the

cavity field. The phase  $\phi$  and consequently the interference between the cavity field and the second excitation pulse depend on two values: The detuning  $\omega_{\text{detuning}}$  and the time delay  $t_{\text{delay}}$  (see Fig. 1(f)).

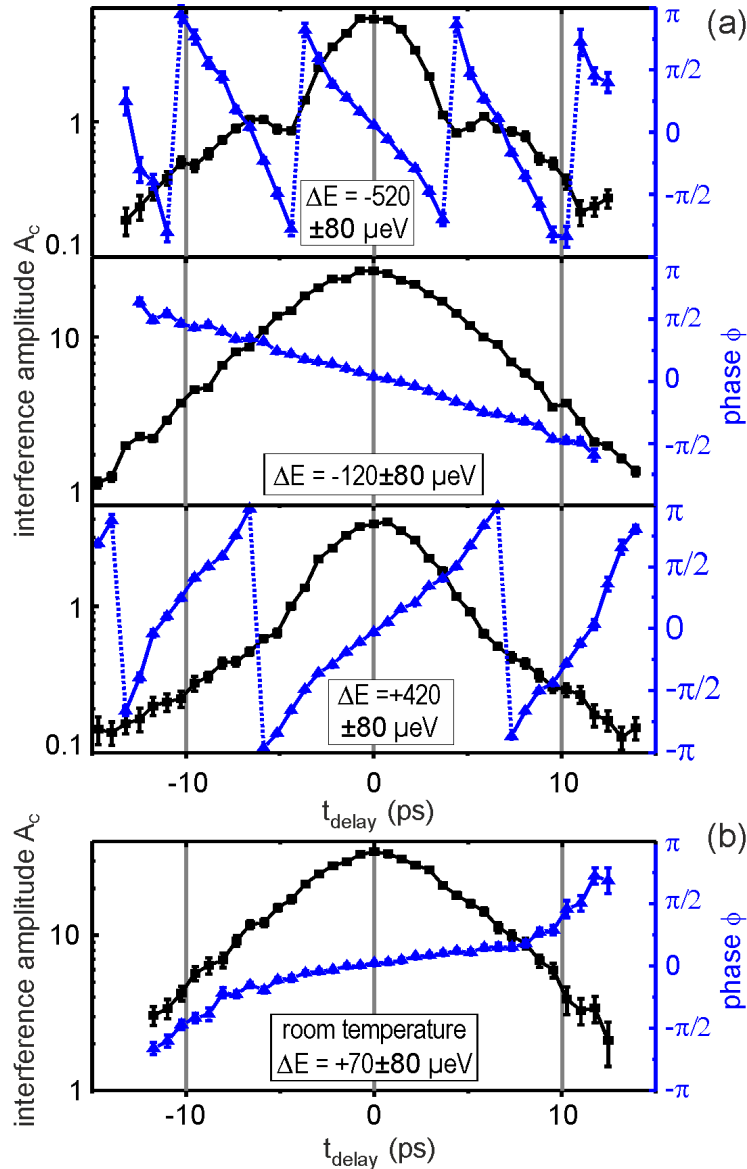


Fig. 3. (a) Experimentally measured interference amplitude and phase for different detunings at  $T = 4.2 \text{ K}$  and an excitation power of  $430 \text{ nW}$ . (b) Room temperature data for weak detuning at an excitation power of  $9.5 \text{ nW}$ .

The response of our detectors, of both the laser power detector and the PhCC photo diode, is much slower than the oscillation frequency. Therefore, the measured signal is proportional to the time average of the squared envelopes  $I_{L,C} \propto \int |g_{L,C}(t)|^2 dt$ . Sections of interference pattern (see Fig. 2(c)) recorded at equal delay steps of  $0.75 \text{ ps}$  and the zoom in of the experimental data (see Fig. 2(d)) are shown for a sample temperature of  $4.2 \text{ K}$  and an

excitation power of 430 nW after the objective lens. The detuning of  $\Delta E = -520 \mu\text{eV}$  was measured by a grating spectrometer with a spectral resolution of  $\pm 80 \mu\text{eV}$ . The interference signal of the laser detector (red curve) as well as the PhCC photo diode PC (black curve) perform sinusoidal oscillations versus time delay (see Fig. 2(d)). The oscillation period is  $T = 2\pi\omega_{c,L}^{-1} \approx 3.2 \text{ fs}$ . The signals of those time averaged measurements are maximal for constructive and minimal for destructive case. For the example shown in Fig. 2(d) the cavity oscillations are shifted in phase by  $\phi = \phi_c - \phi_L$  with respect to the laser signal.

Another important value is the amplitude of the PC oscillations  $A_c$ , measured by the PhCC photo diode. The comparison of the interference patterns between the laser and the PhCC displayed in Fig. 2(c) shows distinct differences between the shapes of the signals. As the laser pattern envelope can be fitted by a  $\text{sech}^2$ -function, the PC signal appears to be modulated and reveals two characteristic dips at  $\pm 4 \text{ ps}$ . One can observe additional minima at  $\pm 11 \text{ ps}$ , by extracting the PC amplitude  $A_c$  and plotting the data logarithmically (see top graph in Fig. 3(a)). By comparing  $A_c$  and the extracted phase function  $\phi$  (blue curve) it becomes apparent that the minima appear under conditions where the phase is equal to  $\pm\pi$ . The observed behavior is discussed in the following section.

## 4. Experimental results and analytic model

### 4.1 Autocorrelation

An interferogram as shown in Fig. 2(c) can be modeled by calculating the autocorrelation function of the laser pulses or the resulting cavity field respectively. For the case of linear WL absorption we measure the E-field autocorrelation which is defined as  $X(t_{\text{delay}}) = \int_{-\infty}^{\infty} |E(t) + E(t - t_{\text{delay}})|^2 dt$ . By taking  $E(t) = \text{Re}\{E_c(t)\exp(i\omega_L t)\}$  with the complex valued cavity field  $E_c(t)$  (slowly varying compared to the carrier frequency  $\omega_L$ ) one can show that

$$X(t_{\text{delay}}) = C + \text{Re}\{\exp(i\omega_L t_{\text{delay}}) \cdot \int_{-\infty}^{\infty} E_c(t) E_c^*(t - t_{\text{delay}}) dt\},$$

where  $C$  is a constant offset. The whole phase and amplitude information of the autocorrelation function  $X(t_{\text{delay}})$  is contained in the remaining integral, which is equal to the autocorrelation of the rotating-frame cavity field  $E_c(t)$ .

### 4.2 Analytic model

The numerically obtained solution for the cavity response  $a(t)$  (see Figs. 1(e) and 1(f)) is a fairly complex function, which contains the detailed signature of the excitation pulse (here for example a  $\text{sech}^2$  function) and the exponential decay caused by cavity ring-down. A simple and more transparent analytic solution can be obtained, if we introduce the following approximation for the cavity response:

$$E_c(t) \approx \begin{cases} e^{+\gamma t}, & t \leq 0 \\ e^{-\gamma t} e^{i\omega_{\text{detuning}} t}, & t \geq 0 \end{cases}$$

The envelope  $g_c(t) = |E_c(t)|$  (solid line) and real part  $\text{Re}\{a(t)\}$  (dashed line) for this approach are shown in Fig. 4(a). Based on this, the autocorrelation function  $X(t_{\text{detuning}}) = \int_{-\infty}^{\infty} E_c(t) E_c^*(t) dt$  can be calculated analytically. The autocorrelation function applied to a complex valued argument is as well complex and Hermitian [19]. It is an even

function with respect to the absolute value and an odd one with respect to the argument. Therefore, it is enough to calculate  $X(t_{\text{detuning}})$  for positive delay times and to expand the function towards negative delay times by using its symmetry properties.

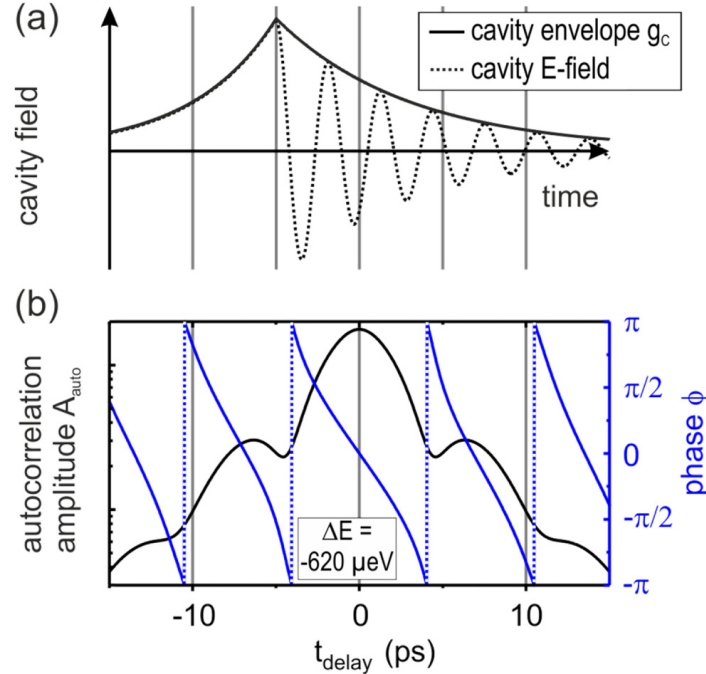


Fig. 4. (a) Cavity response approximated by a complex field amplitude function  $E_C(t)$  showing real part  $\text{Re}\{E_C(t)\}$  and envelope  $g_L(t) = |E_C(t)|$  of the cavity field. (b) Analytic solution for the autocorrelation amplitude and phase using the input parameters shown in Fig. 4(a).

The result for  $t_{\text{delay}} \geq 0$  is

$$X(t_{\text{delay}}) = c_1 e^{-\gamma_1 t_{\text{delay}}} + c_2 e^{-\gamma_2 t_{\text{delay}}} e^{i\omega_{\text{detuning}} t_{\text{delay}}}$$

with the constants

$$c_{1,2} = (2\gamma_{1,2})^{-1} \pm (i\omega_{\text{detuning}} - \gamma_2 + \gamma_1)^{-1}$$

$X(t_{\text{delay}})$  is a sum of two decaying oscillations (consider the rotating frame) with frequencies of the laser and the cavity resonance. The superposition of this oscillations leads to a beating signal (see Fig. 4(b)).

By taking the absolute value or the argument of the complex autocorrelation function we get the amplitude  $A_{\text{auto}}$  or the phase  $\phi_{\text{auto}}$  respectively. The amplitude function was fitted to the experimental data from the top graph in Fig. 3(a). The obtained fit parameters are  $\gamma_1^{-1} = 2.9 \pm 0.3$  ps,  $\gamma_2^{-1} = 4.1 \pm 0.2$  ps and  $\Delta E_{\text{Fit}} = -620 \pm 20$   $\mu\text{eV}$ . The resulting functions for amplitude and phase are shown in Fig. 4(b). They agree almost perfectly with the measured curves shown in Fig. 3(a) (top), which is quite surprising in view of strongly simplified model. The calculated detuning is also very close to the measured value ( $\Delta E = -520 \pm 80$   $\mu\text{eV}$ ).

The modulation of the amplitude function  $A_{auto}$  is caused by the beating between the carrier frequency of the laser and the cavity. Although the amplitude and the phase functions are not periodic, the distance between the side maxima (minima) of  $A_{auto}$  as well as the distance between the points where  $\phi_{auto} = n \cdot \pi$  (or the inflexion points of  $\phi_{auto}$ ) is equal to  $2\pi\omega_{detuning}^{-1}$ . This allows for an experimental determination of the detuning between a reference given by the cavity resonance and unknown laser pulses (unknown frequency).

### 4.3 Experimental results

Figure 3(a) contains three experimental data sets of interference amplitude and phase for different detunings of  $\Delta E = (-520 \mu\text{eV}; -120 \mu\text{eV}; +420 \mu\text{eV})$ . Both functions ( $A_c$  and  $\phi$ ) are strongly influenced by the magnitude of the detuning. In addition to the observations for large detuning ( $\Delta E = -520 \mu\text{eV}$ ), like modulated amplitude function with equidistant extrema, we measure a distinctly different behavior of  $A_c$  for smaller detuning  $\omega_{detuning}$ . As shown in Fig. 3(a) for almost resonant excitation ( $\Delta E = -120 \mu\text{eV}$ ) the amplitude function is completely smooth and a  $\text{sech}^2$ -function can be applied to fit the amplitude shape. The resulting FWHM is two times larger as the width of the laser pulse interferogram. The oscillations of the PC versus time delay can be observed even if the laser signal is decayed. This behavior can be referred to the longer photon lifetime at the cavity resonance and can be further enlarged for higher Q-factors. The measured total PC is enhanced and more than three times higher as for  $\Delta E = -520 \mu\text{eV}$  or  $\Delta E = 420 \mu\text{eV}$  (all curves shown in Fig. 3(a) have been recorded at the same excitation power of 430 nW).

The detuning of  $\Delta E = 420 \mu\text{eV}$  is located between the cases discussed above. The dips at the  $\pm\pi$  transitions of the phase ( $t_{delay} \approx \pm 7$  ps) appear much less pronounced, but they are still characterized by slope changes of the  $A_c$  signal (in full agreement with our analytic theory).

The presented examples show a strong detuning dependence of the amplitude shape. Nevertheless, all discussed cases can be described and fitted by our analytic model. The corresponding detunings obtained from fits are  $\Delta E_{Fit}(-120 \mu\text{eV}) = \pm 200 \pm 60 \mu\text{eV}$  and  $\Delta E_{Fit}(+420 \mu\text{eV}) = \pm 430 \pm 30 \mu\text{eV}$  (the amplitude function has a mirror symmetry and therefore does not include information about the sign of the detuning). In order to describe the rise and fall of the cavity field (see Fig. 4(a)) we have used an exponential model with constants  $\gamma_1$  and  $\gamma_2$ . These constants depend predominantly on the duration of the excitation pulse  $t_{pulse}$  and the Q-factor of the cavity, which remained unchanged for all three measurements. The corresponding fit parameters are also effectively equal:  $\gamma_1^{-1}(-120 \mu\text{eV}) = 2.4 \pm 0.4$  ps,  $\gamma_2^{-1}(-120 \mu\text{eV}) = 4.8 \pm 0.7$  ps and  $\gamma_1^{-1}(+420 \mu\text{eV}) = 2.6 \pm 0.3$  ps,  $\gamma_2^{-1}(+420 \mu\text{eV}) = 4.1 \pm 0.4$  ps. The analytic description of the cavity response agrees amazingly well with our experimental data. This becomes apparent by comparing for example the experimental data shown in Fig. 3(a) for  $\Delta E = -520 \mu\text{eV}$  with the corresponding analytical fit curve shown in Fig. 4(b).

Until now the discussion was concentrated on the amplitude function. The phase evolution for different detunings (see Fig. 3(a)) is more intuitive. An increased detuning leads to a steeper phase evolution and therefore to an increased number of  $\pm\pi$ -transitions. In addition to the magnitude of the detuning one can also distinguish between positive and negative detuning. The sign of the detuning corresponds to the sign of the phase slope (see Fig. 3(a)).

A very interesting behavior is observed for additional measurements at room temperature (see Fig. 3(b)). Amplitude and phase correlate in the same way with the detuning as for  $T = 4.2$  K. The only difference is a much stronger PC response as compared to  $T = 4.2$  K. The data shown in Figs. 3(a) and 3(b) ( $\Delta E = -120 \mu\text{eV}$ ) have been measured at comparable detuning. The PC magnitude is as well comparable, but the measurements were done at different excitation power: 430 nW for  $T = 4.2$  K and 9.5 nW for  $T = 300$  K. The sensitivity at 300 K is 45 times higher than at 4.2 K [16]. This enhancement can be explained by the following effects: (i) better spectral overlap between cavity mode and WL, (ii) thermally enhanced tunneling and thermionic emission [20,21] and (iii) enhanced exciton diffusion length [22,23].

The enhanced sensitivity at room temperature is very interesting for the application of PhCC photo diodes as narrow band photo detectors for cw excitation [16] and also for frequency or phase discrimination for pulsed excitation.

### 5. Coherent control of the cavity field

The coherent control of optical cavities is a promising goal, since it allows for the manipulation of cavity fields and resulting light-matter interactions on timescales below the cavity ring-down limit. An optical cavity excited by a single laser pulse stores the pulse energy for a certain amount of time, which is proportional to the Q-factor of the resonator. During the cavity ring-down the amount of the stored energy continuously decreases. For the case of excitation with two equal but delayed pulses, the remaining cavity excitation caused by the first pulse is always smaller as compared to the excitation by second one. To obtain for example an annihilation of the cavity field created by a first pulse, a suitable second pulse with predefined (reduced) amplitude and phase has to be applied (see Fig. 5(a)).

As shown in Fig. 5(b) for the destructive case, the envelope of the cavity field  $g_L$  vanishes after the second laser pulse has passed. A ring-down behavior can only be observed for the constructive case.

Experimental control of the pulse field strength was achieved by modification of the Michelson interferometer setup. One arm was equipped with a polarizer and an adjustable  $\lambda/2$  plate. After the time delay was set to destructive interference of the cavity field, we have measured the PC response as a function of the pulse fields ratio  $E_2 / E_1$ . On the left side of Fig. 5(c), a PC measurement for a constant delay of  $t_{\text{delay}} = 9.2$  ps at  $T = 4.2$  K and zero detuning is presented. The PC curve exhibits a local minimum at a field ratio of 0.35. This minimum corresponds to a total cancelation of the cavity E-field. A weaker second pulse ( $E_2 / E_1 < 0.35$ ) cannot completely switch off the ring down. For higher field ratios ( $E_2 / E_1 > 0.35$ ) like e.g. equal pulses ( $E_2 / E_1 = 1$ ) the remaining field is overcompensated by the second pulse. Both cases lead to stronger field (envelope) average and thus to higher PC.

The right graph of Fig. 5(c) shows PC data for a shorter delay time ( $t_{\text{delay}} = 7.3$  ps). Coherent control (PC minimum) is achieved for a field ratio  $E_2 / E_1 \approx 0.5$ . This behavior is expected and can be explained by the shorter delay time, which leads to a higher remaining cavity field  $E_1$ .

The presented coherent control of the cavity field can be extended to various cavity geometries and may be very interesting for cavity QED experiments on cavity-quantum dot systems.

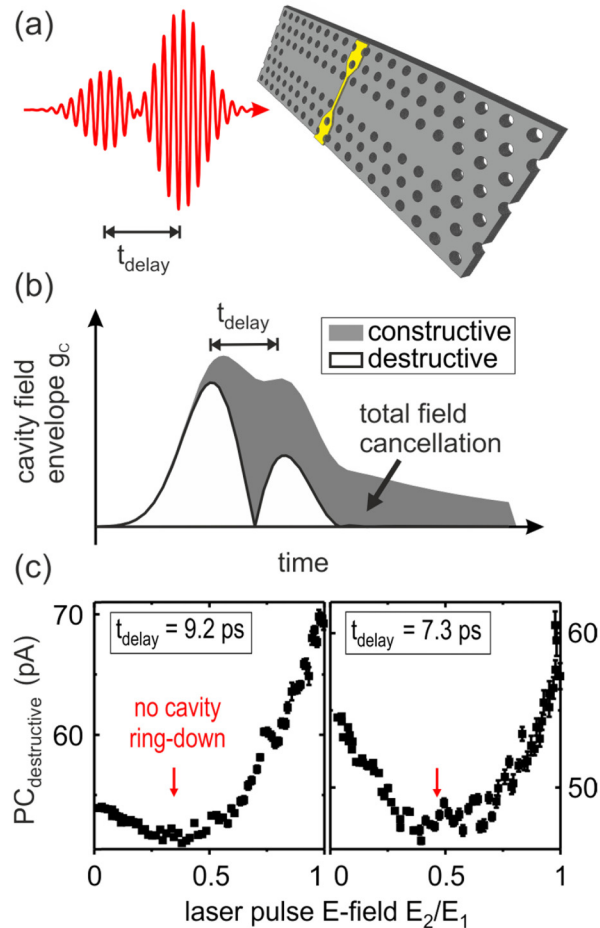


Fig. 5. (a) PhCC excited by two destructively interfering delayed pulses. The second pulse is attenuated with respect to the first pulse. (b) Time dependent cavity field envelopes for constructive and destructive interference. The second pulse cancels the cavity ring-down. (c) Experimental observation of coherent control of the cavity field for pulses delayed by 9.2 ps (left) and 7.3 ps (right). The PC minima correspond to the conditions of cavity ring-down cancellation.

## 6. Conclusion

We have presented a phase sensitive analysis of the cavity field in a PhCC by two pulse interference. The interference patterns can be explained and fitted by a simple, but accurate analytic model, which can also describe the E-field autocorrelation behavior for different detuning scenarios. The measured interference amplitude and phase shift between the cavity and laser field allows for an enhanced frequency discrimination, due to the availability of phase information.

For the case of detuning, the cavity field starts to oscillate with the laser frequency. After the excitation pulse has vanished, the cavity enters the ring down regime, during which the frequency is given by the bare cavity frequency. This corresponds to a frequency chirp, which can be controlled in sign and magnitude by the adjustment of the detuning. This concept may be in particular interesting for the coherent state preparation in quantum dot – cavity systems. Advanced excitation schemes like the adiabatic passage [24–26] could be tailored by selecting specific conditions of detuning between cavity, quantum dot and laser. A positive chirp could be realized for example by a laser pulse with a frequency, which is

red-shifted with respect to the cavity mode frequency, with the quantum dot frequency in between laser and cavity. For such a configuration the quantum dot would be exposed to a cavity field, which sweeps from negative to positive detuning over the quantum dot resonance frequency.

Double pulse excitation and the adjustment of the amplitude and phase of second laser pulse during cavity ring-down further allows for the coherent control of the cavity field.

The experimental proof and verification of the above described phenomena became possible by an electric detection scheme, which employs planar photonic crystal microcavity photo diodes with metallic Schottky contacts in the defect region of the resonator. The applied photo current detection was shown to work also efficiently at room temperature, which makes electrically contacted microcavities attractive for real world applications. The general concept can also be applied to different cavity geometries or material systems.

In summary we believe that the phase sensitive manipulation and analysis of cavity fields as presented here is important for the further development of ultrafast cavity physics and its applications both for real world room temperature devices and for photonic quantum technologies.

### **Funding**

Deutsche Forschungsgemeinschaft (DFG) (Research Training Group 1464, SFB-TRR 142); German Federal Ministry of Education and Research (BMBF) (16KIS0109, 16KIS0114).